Probing new spin-independent interactions through precision spectroscopy in atoms with few electrons

PHYSICAL REVIEW D **96,** 115002 (2017)

Probing new spin-independent interactions through precision spectroscopy in atoms with few electrons

Cédric Delaunay,[1] Claudia Frugiuele,[2] Elina Fuchs,[2] and Yotam Soreq[3]

[1]*Laboratoire d'Annecy-le-Vieux de Physique Théorique LAPTh, CNRS-USMB, BP 110 Annecy-le-Vieux, F-74941 Annecy, France*

[2]*Department of Particle Physics and Astrophysics, Weizmann Institute of Science, Rehovot 7610001, Israel*

[3]*Center for Theoretical Physics, Massachusetts Institute of Technology, Cambridge, Massachusetts 02139, USA*

(Received 25 September 2017; published 5 December 2017)

The very high precision of current measurements and theory predictions of spectral lines in few-electron atoms allows us to efficiently probe the existence of exotic forces between electrons, neutrons and protons. We investigate the sensitivity to new spin-independent interactions in transition frequencies (and their isotopic shifts) of hydrogen, helium and some heliumlike ions. We find that present data probe new regions of the force-carrier couplings to electrons and neutrons around the MeV mass range. We also find that, below few keV, the sensitivity to the electron coupling in precision spectroscopy of helium and positronium is comparable to that of the anomalous magnetic moment of the electron. Finally, we interpret our results in the dark-photon model where a new gauge boson is kinetically mixed with the photon. There, we show that helium transitions, combined with the anomalous magnetic moment of the electron, provide the strongest indirect bound from laboratory experiments above 100 keV.

DOI: 10.1103/PhysRevD.96.115002

I. INTRODUCTION

Fundamental interactions of known elementary particles are well described by the Standard Model (SM) of particle physics. Nevertheless, the SM cannot be the complete description of Nature since it does not account for neutrino oscillations, does not provide a viable dark matter candidate and cannot explain the baryon asymmetry of the Universe. Moreover, the SM suffers from several hierarchy problems, such as the stability of the Higgs mass to quantum corrections and the strong CP problem. In addition, it contains intriguing puzzles related to the observed large hierarchies in the charged fermion masses and quark mixing angles. However, non of these pending issues which call for new physics (NP) beyond the SM indicate a specific energy scale at which the associated NP phenomena will manifest themselves. Hence, a broad experimental program must be pursued.

While accelator-based experiments search directly for new particles over many orders of the mass and couplings, precision low-energy measurements may also reveal indirectly in a complementary approach the existence of new phenomena. Precise atomic physics table-top experiments are promising in this regard. For example, observables which violate discrete symmetries of QED, as in parity-violating transitions [1–8], are a powerful tool to probe NP [9].

Parity-conserving transitions are also interesting probes of NP which, however, require higher theoretical control. Frequency measurements of narrow atomic transitions in heavy elements are possible within a few $\times 10^{-16}$ relative accuracy [10,11] thanks to the optical frequency comb technique [12,13]. Moreover, the experimental uncertainty in some systems now reaches the 10^{-18} level [14,15], thus indicating the possibility of significant improvement in the near future. A limitation in translating the experimental precision to a bound on NP is the theory uncertainty, which is by far larger than the experimental precision. However, the high accuracy achieved in frequency measurements of narrow atomic transitions in heavy elements can be exploited to probe NP provided new observables largely insensitive to theory uncertainties are identified. For example, Refs. [16–19] proposed to bound new interactions between neutrons and electrons by testing linearity of King plots [20] of isotope shift (IS) measurements.

The situation is different for atoms and ions with few electrons and a small number of nucleons. There, QED calculations are carried out to high accuracy. For instance, low excited states in helium can be calculated up to $\mathcal{O}(\alpha^6)$ corrections, which yields theoretical predictions often more accurate than the measurements, see e.g. Refs. [21,22]. In addition, nuclear finite size effects are also well described thanks to the extraction of the nuclear radius from electron scattering experiments and muonic atom spectroscopy. This allows us to directly compare theory and experiment in order to probe NP interactions [23–26].

In this work we derive new limits on spin-independent NP interactions between the proton/neutron and the electron from optical frequency measurements, as well as from frequency shifts between different isotopes, in hydrogen and helium atoms, heliumlike ions such as lithium and nitrogen. In addition, we constrain new electron-electron interactions via precision spectroscopy of helium and

positronium atoms. We compare the resulting bounds on the product of the electron and neutron couplings and on the electron coupling separately, with existing indirect constraints and future prospects from IS measurement in heavier systems with many electrons. Furthermore, we perform global fits using all available transitions to constrain simultaneously the electron, neutron and proton couplings in a model-independent way. Finally, as a phenomenological application, we interpret the bounds within the dark photon model.

II. CONSTRAINING NEW SPIN-INDEPENDENT INTERACTIONS IN ATOMS

Consider a new force mediated by a boson ϕ of mass m_ϕ and spin $s = 0, 1, 2$ with spin-independent couplings to the electron, proton and neutron y_e, y_p and y_n, respectively. At atomic energies, the exchange of ϕ is described by an effective potential between a nucleus N of charge Z and mass number A and its bound electrons as

$$V_N(r) = \frac{(-1)^{s+1}}{4\pi} y_e y_N \frac{e^{-m_\phi r}}{r}, \tag{1}$$

where $y_N \equiv y_p Z + (A - Z) y_n$ and r is the electron-nucleus distance.

For atoms with more than one electron, like helium, an effective potential between electron pairs is also induced

$$V_e(r_{12}) = (-1)^{s+1} \frac{y_e^2}{4\pi} \frac{e^{-m_\phi r_{12}}}{r_{12}}, \tag{2}$$

where $r_{12} \equiv |\vec{r}_1 - \vec{r}_2|$ is the distance between electron 1 and electron 2, with $\vec{r}_1$, $\vec{r}_2$ describing their positions relative to the nucleus.

The total frequency shift induced by the above potentials for a transition i between atomic states a and b (with $E_b > E_a$) is described by first-order perturbation theory as

$$\delta_{\rm NP}\nu_i^A = (-1)^{s+1}(y_e y_N X_i + y_e^2 Y_i), \tag{3}$$

where X_i and Y_i are overlap integrals with the electronic wave functions depending only on the ϕ boson mass. In this paper, we focus on electronic transitions in heliumlike and hydrogen atoms, for which the X_i and Y_i functions are calculated within first-order perturbation theory using nonrelativistic wave functions as detailed in Appendices B and C. While QED calculations rely on much more sophisticated wave functions, the use of the nonrelativistic ones is a sufficient approximation to the dominant NP effects. Helium wave functions are very well approximated by antisymmetrized combinations of hydrogenic wave functions with effective nuclear charges accounting for the electronic screening [27], except for the $2S$ spin-singlet state where an accurate description of the interelectron repulsion requires the use of Hylleraas functions [28,29].

Taking into account the NP contribution in Eq. (3), the theory prediction for the frequency of an electronic transition i in an isotope A is given by

$$\nu_i^A = \nu_{i,0}^A + F_i \langle r^2 \rangle_A + \delta_{\rm NP}\nu_i^A, \tag{4}$$

where $\nu_{i,0}^A$ is the dominant contribution calculated in the pointlike nucleus limit (including spin effects and nuclear polarizability), whereas the second term describes the leading finite nuclear size effects, $\langle r^2 \rangle_A$ being the nuclear charge radius squared and F_i is the field-shift (FS) constant. The IS between two isotopes A and A' for this transition is then described as

$$\nu_i^{A,A'} = \nu_{i,0}^{A,A'} + F_i \delta\langle r^2 \rangle_{A,A'} + y_e y_n X_i (A - A'), \tag{5}$$

where $\nu_i^{A,A'} \equiv \nu_i^A - \nu_i^{A'}$ and $\delta\langle r^2 \rangle_{A,A'} \equiv \langle r^2 \rangle_A - \langle r^2 \rangle_{A'}$. Higher-order effects of nuclear charge radius and finite magnetic radius are not resolvable by the current experimental accuracy [21,30] and are therefore omitted in Eqs. (4) and (5).

Absolute frequencies and IS in hydrogen and helium are calculated to high accuracy in the limit of pointlike nuclei. However, the full theoretical prediction is often limited by the uncertainty related to the finite nuclear size effects. For a comparison between the experimental value and the QED prediction in the point-nucleus limit, we define

$$\Delta_i^A \equiv \nu_{i,\rm exp}^A - \nu_{i,0}^A. \tag{6}$$

The NP contribution generically depends on the three coupling constants, y_e, y_p, and y_n, and the mediator mass, m_ϕ. At fixed m_ϕ the product $y_e y_n$ can be probed independently of y_p from a single IS measurement (for any transition i) using Eq. (5)

$$y_e y_n = \frac{\Delta_i^{A,A'} - F_i \delta\langle r^2 \rangle_{A,A'}}{X_i (A - A')}, \tag{7}$$

where $\Delta_i^{A,A'} \equiv \Delta_i^A - \Delta_i^{A'}$ using Eq. (6). Hence the NP bound depends on the change in the mean-square nuclear charge radius, $\delta\langle r^2 \rangle_{A,A'}$, which is measured either in electron scattering or in muonic atom spectroscopy experiments. Whenever applicable, the latter typically yields much more precise values of the charge radii. In principle, the charge radius determination via electron scattering may be affected by NP. However, we find that NP is only noticeable there for large coupling values that are already excluded by more sensitive probes. Hence the charge radius extraction from electron scattering cannot be contaminated by NP. Muonic atom spectroscopy measurements are more sensitive to NP contributions, especially in the keV–MeV mass range, and existing constraints on the $y_\mu y_n$ coupling product do not rule out the possibility of NP contaminations in this region

[31–33]. Therefore, for simplicity we will henceforth assume $y_\mu = 0$.

Alternatively, the charge radius dependence can be eliminated using an IS measurement in a second transition, yielding

$$y_e y_n = \frac{F_2 \Delta_1^{A,A'} - F_1 \Delta_2^{A,A'}}{(F_2 X_1 - F_1 X_2)(A - A')}, \tag{8}$$

which, besides $X_{1,2}$, depends only on quantities known theoretically with high accuracy, namely F_2/F_1 and $\nu_{i,0}^{A,A'}$. The main drawback of Eq. (8) relative to Eq. (7) is the possible loss of sensitivity when $(F_2 X_1 - F_1 X_2) \to 0$ [16,19]. The latter is rather severe *for all* m_ϕ when close-by transitions with $F_1 \approx F_2$ and $X_1 \approx X_2$ are used, for example in transitions involving different states of the same fine-structure multiplet. Another disadvantage of Eq. (8) is represented by how rapidly the sensitivity to $y_e y_n$ weakens at large mass. While $X_i \propto m_\phi^{-2}$ above $m_\phi \sim \mathcal{O}(10\ \mathrm{keV})$, this leading term cancels out in the difference $(F_2 X_1 - F_1 X_2) \propto m_\phi^{-3}$ [19]. Equation (8) bears resemblance to the method proposed in Ref. [19] for heavy elements. However, there, the less accurate theory calculations for $\nu_{i,0}^{A,A'}$ are traded for IS measurements between two additional isotope pairs.

NP contributions to the electron-electron and electron-proton interactions cancel out to first approximation in the IS. Thus, they can be probed more efficiently in absolute frequency measurements, despite the lower absolute accuracy. Helium transitions are sensitive to both kinds of interaction. In fact a combination of two frequency measurements can resolve the $y_e y_N$ and y_e^2 coupling products, thanks to transition-dependent X_i, Y_i constants in Eq. (3). Hydrogen frequencies are sensitive to electron-proton interactions and have been used previously to probe $y_e y_p$ [23–25]. However, presently unresolved issues related to the well-known proton radius puzzle [34,35] limits the application of hydrogen spectroscopy for constraining new atomic forces. Therefore, we will not use absolute spectroscopy measurements of hydrogen or deuterium as a probe of NP. Instead, we will consider hydrogen-deuterium IS spectroscopy since in this case there is no tension between $\delta\langle r^2\rangle$ values extracted from electronic and muonic measurements [36].

III. BOUNDS FROM ISOTOPE SHIFT MEASUREMENTS

Let us first discuss probes of new electron-neutron interactions. We focus here on spectroscopic probes based on IS measurements in helium, heliumlike and hydrogen/deuterium atoms. The comparison of theory to experiment directly probes $y_e y_n$ independently of the presence of a NP coupling to protons. As shown in Table I (a full list of our input values is given in Appendix A), the theory uncertainty (in the point-like nucleus limit) is currently smaller than the experimental error for transitions involving low excited states, and the sensitivity to NP is limited by the experimental determination of charge radius differences. Our results are summarized in Fig. 1 which show the best constraints on

TABLE I. Allowed NP contributions $\delta_{\mathrm{NP}}\nu$ for the most accurate IS measurements in helium and hydrogen isotopes, along with the standard uncertainties from experiment, $\sigma_{\nu_{\mathrm{exp}}}$, QED calculation (point-nucleus limit, σ_{ν_0}) and charge radius difference extracted from electron-scattering data, $\sigma_{\delta\langle r^2\rangle}$. Only for $2S - 12D$ in H/D, σ_{ν_0} refers to the complete theory prediction including the FS. All numbers are in kHz. For references and input values, see Tables III and IV.

Isotopes	Transition	$\delta_{\mathrm{NP}}\nu$	$\sigma_{\nu_{\mathrm{exp}}}$	σ_{ν_0}	$\sigma_{\delta\langle r^2\rangle}$
^{3}He/^{4}He	$2^1S - 2^3S$	$+9 \pm 14$	2.4	0.19	14
	$2^3P - 2S$	-2 ± 78	3.3	0.9	78
H/D	$1S - 2S$	$+76 \pm 61$	0.02	0.9	61
	$2S - 12D$	$+1.2 \pm 10$	9.3	4.2	

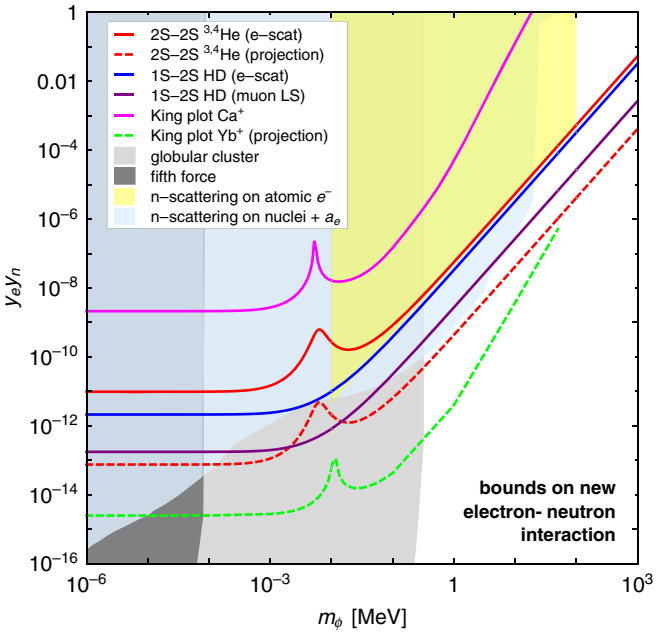

FIG. 1. Summary of the indirect constraints on a new electron-neutron interaction: isotope shift spectroscopy of helium and hydrogen/deuterium (this work) with the charge radius determined from electron scattering ("e-scat" or Lamb shift in muonic atoms ("muon LS"; comparison with King plot analyses of IS in heavy atoms (Ca^+, Yb^+) [19,37], fifth force experiments [38,39], electron-neutron scattering [40], neutron-nucleus scattering [41–44] combined [19] with a_e, and globular cluster [45]. The existing bounds are in solid lines, while the projections are in dashed lines. The He projection assumes a combined theory and experimental uncertainty of 100 Hz; the Yb^+ projection assumes King linearity at 1 Hz.

$y_e y_n$, as a function of the mediator mass, arising from transitions in hydrogen and helium(-like) atoms.

For comparison, we also show constraints derived from King linearity in heavy atoms [19] and from other (nonatomic) observables. Those include laboratory constraints resulting from the anomalous magnetic moment of the electron $a_e \equiv (g-2)_e/2$ [46,47], neutron scattering on atomic electrons [40] or nuclei [41–44] and fifth force experiments [38,39], as well as astrophysical constraints from SN 987a [48] and globular clusters [45,49–52]. Note that also spectroscopy in molecular ions and antiprotonic helium constrains spin-independent interactions of nucleons [53–56], but it results in weaker bounds than from neutron scattering and is therefore not shown in Fig. 1. Some of these constraints can be evaded in specific models [57–61]. We notice that bounds from few-electron atoms provide the strongest (indirect) constraints in the region above 300 keV where astrophysical bounds lose sensitivity. Note, however, that direct constraints (not shown here) also exist, which are particularly sensitive for $m_\phi > 1$ MeV. Yet, they strongly depend on the assumed branching ratios for relevant ϕ decay modes, see e.g. Ref. [62] for a review. In the near future a higher sensitivity to NP is still expected in the King linearity test of Yb^+ [19] compared to few-electron atom spectroscopy, despite the projected improvements in helium transitions. In addition, it is interesting to notice that very light scalar spin-independent interactions can be tested by macroscopic systems, see e.g. [63–68]. In the following subsections, we discuss in detail the bounds obtained from IS measurements in helium, heliumlike ions and hydrogen/deuterium atoms.

A. Helium and heliumlike isotope shifts

We derive here IS bounds using precision spectroscopy in two-electron atoms. This includes constraints from measurements in helium and heliumlike lithium and nitrogen ions, all of which are presented in Fig. 2, while the strongest one is also reported in Fig. 1 for comparison with constraints from other atoms and different sources.

The most accurate IS in helium are measured within a few kHz uncertainty between $A = 3$, 4 for the $2^1S - 2^3S$ [69] and $2^3P - 2^3S$ [70,71] transitions around 1557 nm and 1083 nm, respectively. While QED calculations in the point-nucleus limit reached sub-kHz accuracy, the theory prediction for the IS is limited by the charge radius difference $\delta\langle r^2\rangle_{3,4}$ [21]. The latter can be extracted within a few percent from e-He scattering data [72],

$$\delta\langle r^2\rangle_{3,4}^{\text{e-scat}} = (1.067 \pm 0.065)\ \text{fm}^2. \tag{9}$$

Using Eq. (9) as an input for the theory predictions of He IS yields a good agreement between theory and experiment for both transitions, thus allowing to constrain NP electron-neutron interactions.

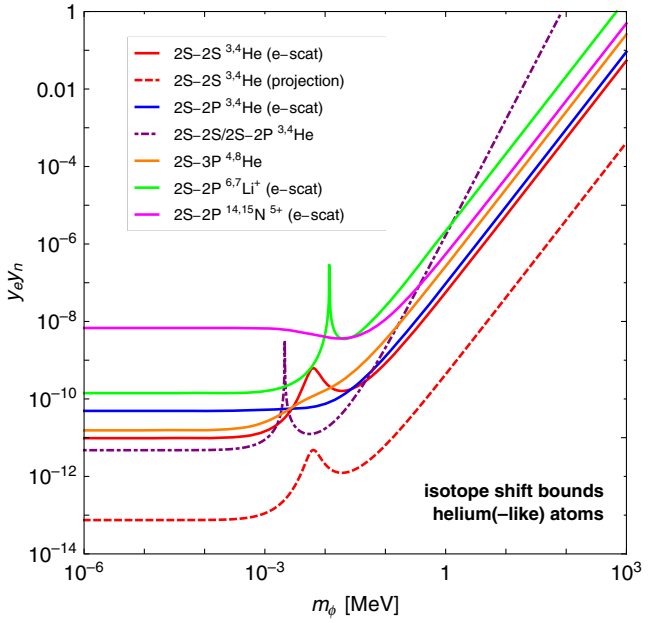

FIG. 2. Isotope shift bounds on new electron-neutron interaction from helium spectroscopy. The solid red and blue lines are the limits from the 1557 nm and 1083 nm transitions, respectively, using the charge radii from e-He scattering. The dotted-dashed purple line is an illustration of the potential limit obtained by combining the two transitions (due to a 4σ tension, see text for details). The solid orange line is the upper bound derived from IS in unstable isotopes. The dashed red line represents the projected sensitivity with the 1557 nm transition using charge radii from muonic helium and assuming a combined experimental and theory uncertainty of 100 Hz.

A higher sensitivity could be reached by combining the two transitions in order to eliminate $\delta\langle r^2\rangle_{3,4}$. In that case, Eq. (8) results in

$$y_e y_n \approx \frac{(-51 \pm 14)\ \text{kHz}}{(5.7X_{1557} - X_{1083})}, \tag{10}$$

which is $\sim 4\sigma$ away from zero. Thus, it is not justified, given such a disagreement, to use the above to set limits on NP. Note, however, that this large deviation is the mere consequence of a known tension between the two transitions which may originate from underestimated uncertainties [21]. Despite this circumstance, it remains interesting to observe that in the case that the tension will be resolved by refined QED calculations and/or measurements, the expected sensitivity to $y_e y_n$ is stronger by a factor ~ 6 relative to the use of $\delta\langle r^2\rangle_{3,4}^{\text{e-scat}}$. In the (yet implausible) event that the above deviation is an evidence for a new electron-neutron interaction, the latter should be visible in other atomic systems. For instance, Eq. (10) would imply a violation of King linearity in ytterbium ion clock transitions at the $\mathcal{O}(100\ \text{Hz})$ level [19].

Alternatively, $\delta\langle r^2\rangle_{3,4}$ can be extracted with high accuracy from muonic helium spectroscopy. The CREMA collaboration is currently conducting Lamb shift

measurements in muonic He^+ aiming at a determination of ^{3,4}He charge radii with a relative uncertainty of 3×10^{-4} [73]. Assuming this will result in a $\delta\langle r^2\rangle_{3,4}$ value consistent with e-He scattering and (electronic) helium spectroscopic data, the sensitivity to NP will hence be limited by the experimental accuracy in helium IS measurements. Moreover, future IS measurements in the $2^1S - 2^3S$ transition down to $\mathcal{O}(100\ \text{Hz})$ precision are expected [74], with a comparable theory improvement. Hence, this would potentially improve sensitivity to NP effects for that transition by two orders of magnitude. As shown in Fig. 1, this is still weaker than the sensitivity expected from King linearity violation in ytterbium ions, except for $m_\phi \gtrsim 10$ MeV due to the different scaling of the bound with the mediator mass (m_ϕ^2 vs m_ϕ^3).

Precision measurements are also achievable in heavier (unstable) helium isotopes. For instance, IS between $A = 4$ and $A = 6, 8$ isotopes for the $2^2S - 3^3P$ transition (389 nm) are measured with ∼100 kHz accuracy [75]. However, the situation is different here since there is no independent measurement of the ^{6,8}He charge radii and the FS cannot be reliably predicted for the 389 nm transition. Nevertheless one can still derive an upper bound on NP by saturating the difference between theory (assuming a point-like nucleus) and experiment, which corresponds to setting $\delta\langle r^2\rangle_{AA'} = 0$ in Eq. (7). Since $\Delta_{389}^{8,4} = -0.918$ MHz [75], the NP contribution is not strongly constrained. Yet, the resulting bound on $y_e y_n$ is strengthened by a factor of $A - A' = 4$ which makes it comparable to the IS bound from the 1083 nm transition. An order of magnitude improvement could be obtained with an independent determination of the charge radii of $A = 6, 8$ isotope of helium.

Finally, IS in heliumlike ions are also well measured. The highest accuracy is obtained in singly-ionized lithium [76] and five-times ionized nitrogen [77]. The measured frequency shifts are between $A = 6, 7$ in the $2^3S - 2^3P$ transition for Li^+, and between $A = 14, 15$ in the $2^1S - 2^3P$ transition for N^{5+}. We rely on the theory predictions used in the quoted references. This assumes nuclear charge radii determined from electron-scattering data [78] with a relative accuracy of ∼2% for lithium and from electron-scattering data [79] and muonic x-ray line measurements [80] with ∼0.5% for nitrogen. The resulting bounds are weaker than the ones from helium. Further precision measurements with heliumlike boron and carbon ions are also underway [21].

B. Hydrogen-deuterium shifts

Hydrogen-deuterium shifts are complementary probes of new electron-neutron interactions. The most accurate IS measurement is for the $1S - 2S$ transition (121.6 nm), with $\sim 10^{-11}$ relative uncertainty [81,82]. The QED calculation is less precise by a factor of ∼60, being equally limited by the experimental value of the proton-to-electron and deuteron-to-electron mass ratios as well as higher-order corrections to the Lamb shift and nuclear polarizability [81]. Additional IS measurements exist with lower precision, including the $2S - nS/D$ transition series for $n = 8, 12$ states [83–85], and the frequency differences [86]

$$\nu_{\text{LS}}^L \equiv \nu_{2S-4L} - \frac{1}{4}\nu_{1S-2S}, \tag{11}$$

with $L = S, D$. The latter is constructed such that the leading contribution from Coulomb-like potentials cancels out, thus making it directly sensitive to Lamb shift (LS) corrections. As a result, ν_{LS}^L becomes less sensitive to NP with an interaction range longer than the atomic size $\sim a_0 = (\alpha m_e)^{-1} \approx (4\ \text{keV})^{-1}$. Since all transitions in the $2S - nS/D$ series have comparable sensitivity to NP, we consider only the $2S - 12D$ transition for illustration.

Here again, the FS contributions are least known theoretically as they are limited by the charge radius difference $\delta\langle r^2\rangle_{2,1}$ between the deuteron and the proton. The latter can be extracted either from electron scattering data,[1] which yields [88]

$$\delta\langle r^2\rangle_{2,1}^{\text{e-scat}} = (3.764 \pm 0.045)\ \text{fm}^2, \tag{12}$$

or muonic hydrogen/deuterium spectroscopy [36]

$$\delta\langle r^2\rangle_{2,1}^{\mu} = (3.8112 \pm 0.0034)\ \text{fm}^2. \tag{13}$$

Note that the charge radius differences in Eqs. (12) and (13) are consistent within uncertainties, despite the (still puzzling) significant discrepancies between muonic and electronic determinations of the proton [34,35] and deuteron [36] radii. Using $\delta\langle r^2\rangle_{2,1}^{\mu}$ to predict the FS contribution yields a sensitivity to NP larger by a factor ∼13 relative to $\delta\langle r^2\rangle_{2,1}^{\text{e-scat}}$, assuming the radii extraction from muonic spectroscopy is not affected by a possible NP coupling to muons.

The IS bounds on a new electron-neutron interaction from hydrogen/deuterium are summarized in Fig. 3.

IV. BOUNDS FROM ABSOLUTE FREQUENCY MEASUREMENTS

While IS are only sensitive to electron-neutron interactions, absolute frequencies can also probe the electron-proton and, in atoms with more than one electron or in positronium, electron-electron interactions. As we discussed above, by measuring two transitions one can extract y_e and y_N separately, and the combination with the IS data will also allow for a separation of y_p from y_n.

In case ϕ couples both to protons and neutrons with a similar strength, as in a Higgs portal or gauged $B - L$, the sensitivity to probe NP with IS is expected to be stronger than from the absolute frequency measurements. This can

[1]We use here the proton radius value extracted from the so-called Mainz data [87].

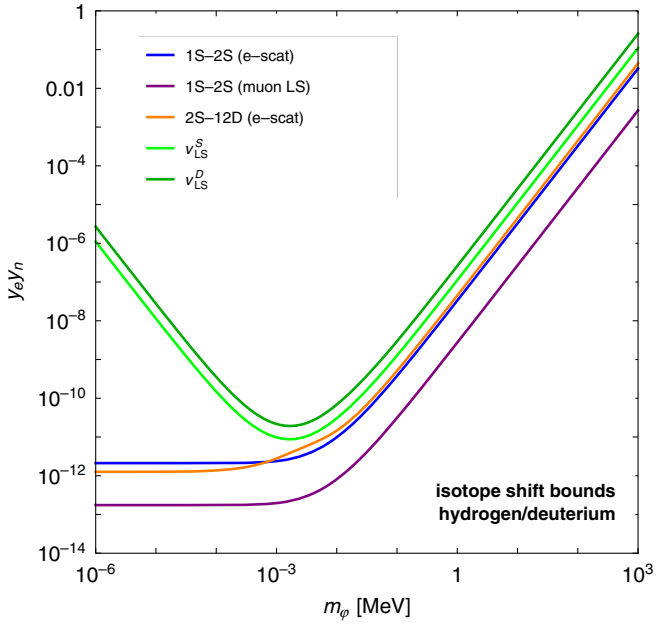

FIG. 3. Isotope shift bounds on new electron-neutron interaction from hydrogen/deuterium spectroscopy. The blue (purple) line is the limit from the $1S-2S$ transition using charge radii from electron scattering (muonic spectroscopy). The orange and green lines are limits derived from the $2S-12D$ transition and the $\nu_{LS}^{S,D}$ observables, respectively, using electron-scattering data. See text for details.

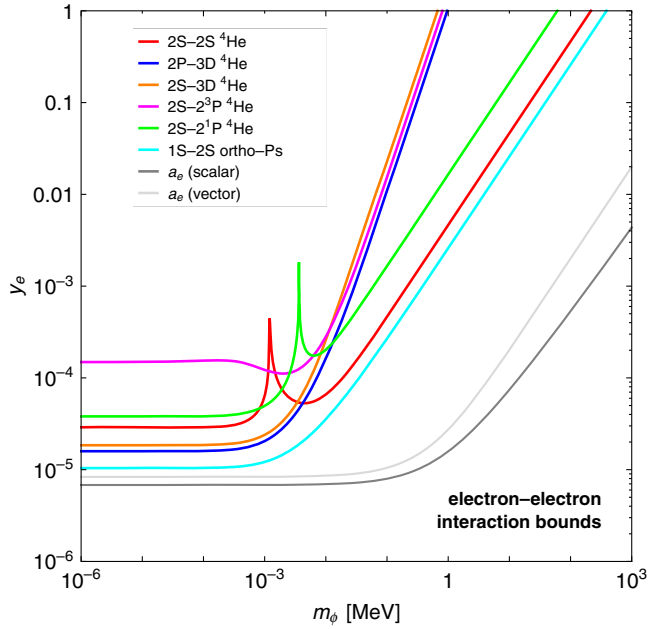

FIG. 4. The upper bound on y_e as function of m_ϕ from $1^3S_1-2^3S_1$ in positronium [89,90] (cyan), helium data [21] and a comparison to electron magnetic moment, a_e, for a scalar (dark gray) and vector (light gray).

be understood as follows. In light atoms, the NP contributions to the IS and to the absolute frequency are of the same order. However, typically the absolute accuracy of IS data (theory and experiment) is better by at least an order of magnitude than the absolute frequency data, see Appendix A. Thus, for $y_n \approx y_p$ IS measurements are a more sensitive to NP than the absolute frequencies.

It is important to distinguish between the case of a generic new force coupled to the electron and to the nucleus (including the proton) and the case of a dark photon (kinetic mixing) where the charges are proportional to the electric charges and a more careful treatment of the definition of the electromagnetic coupling, α, is required, see Ref. [25].

A. Bounds on y_e from helium and positronium

The electron-electron interaction can be probed in atoms with more than one electron, the simplest is helium, or in purely electronic systems such as positronium. Starting with the positronium, the $1^3S_1-2^3S_1$ interval is measured at the 10^{-9} level [89] in a agreement with the theory prediction of Ref. [90]. For helium we combine all the transitions that are given in Table II of Ref. [21], where the agreement between theory and experiment is better than 2σ; the full list is given in Appendix A. Thus, we use the above to put upper bounds on y_e as function of the force-carrier mass m_ϕ. The results are presented in Fig. 4, where we also added the constraint from the electron magnetic moment, a_e, for comparison. This shows that a_e is still the strongest probe among the three. Yet the ϕ contribution to a_e enters only at the loop level which makes it more prone to cancelation against additional contributions from other states present in a complete NP model. Note that the helium bounds in Fig. 4 are evaluated by assuming no electron-nucleus interactions. We have verified that marginalizing over the latter does not significantly change the bounds. The bounds from positronium and helium are comparable and below few keV are weaker than the bound from a_e only a factor of few.

B. Model-independent bounds on y_e, y_p and y_e

Here we combine observables from different atoms to probe the NP couplings y_p, y_n and y_e independently. In order to do so we perform a global fit based on a χ^2 function constructed from IS in hydrogen and helium as well as absolute transition frequencies in helium. Our χ^2 is composed of the 2^1S-2^3S and 2^3P-2S IS between ^{3}He and ^{4}He, the helium/deuterium IS in the $1S-2S$ transition and the ν_{LS}^{S} observable, and the absolute frequencies considered in Sec. IV A. We present in Fig. 5, the 95% CL contours in the y_e-y_p and y_e-y_n planes for several values of m_ϕ. For each pair of couplings, we marginalize over the third coupling y_n and y_p, respectively. The generic shape of the bounds is understood as follows. Since the overlap integrals X_i, Y_i for electron-nucleus and electron-electron interactions are of comparable order when $y_{p,n} \gtrsim y_e$, absolute frequencies and IS constrain the products $y_e y_p$ and $y_e y_n$, respectively, leading to contours at 45 degrees. The latter are then truncated

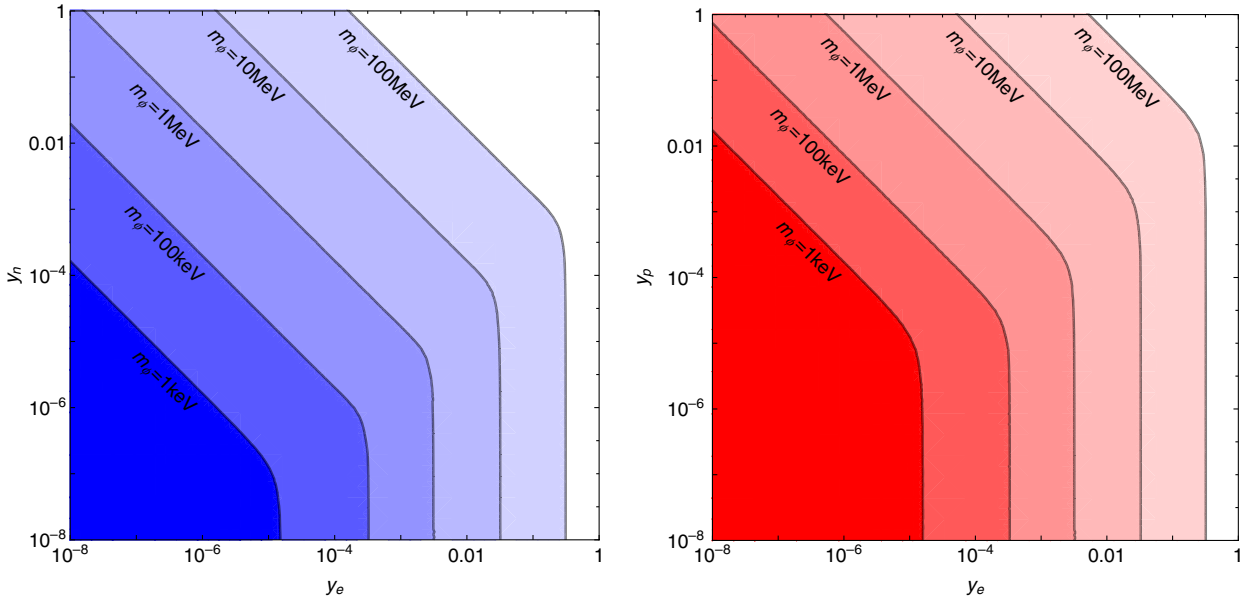

FIG. 5. The allowed region 95% CL contours for fixed mediator mass (as indicated in the plot) from the global χ^2 analysis of helium and hydrogen absolute frequencies as well as their isotope shifts. The left (right) panel shows contours of y_n (y_p) vs y_e, marginalizing over y_p (y_n).

once y_e reaches a large value (typically $y_e \gtrsim y_{p,n}$) so that the y_e^2 term dominates the NP contribution to absolute frequencies in helium and the bounds become independent of y_p or y_n. Note that helium absolute frequencies are in principle sensitive to a possible relative sign between the nuclear and the electron couplings. We checked that either sign yields very similar bounds and thus, for simplicity, we present global-fit results for positive couplings only.

C. Atomic bounds on kinetic mixing

For the sake of illustration, we apply now our result to a specific NP model, that of a kinetically mixed massive gauge boson, the dark photon, denoted as A' [91]. As a result of the mixing between the photon and the dark photon, A' couples to the electromagnetic current, and its couplings to the protons, electrons and neutrons are $y_{p,n,e} = \epsilon e, 0, -\epsilon e$, respectively, where e is the QED gauge coupling constant and ϵ is a mixing parameter. Since all A' couplings are determined by a single parameter, a single atomic transition would suffice to probe it. However, when $m_{A'} \lesssim 1/a_0$, the dark photon induces a $1/r$ atomic potential which is not distinguishable from the Coulomb one and the A' effect is a mere redefinition of the fine-structure constant, $\alpha \to (1+\epsilon^2)\alpha$. Hence, in this regime, we need at least two observables to probe the dark photon, one of them being used to fix α. We follow here the procedure of Ref. [25] and combine either two atomic transitions together or one transition with a_e, the anomalous magnetic moment of the electron. Figure 6 shows the 95% CL bounds that we derived from helium and positronium, each combined with a_e, as well as existing bounds from hydrogen spectroscopy [23–25]. We find that helium and positronium

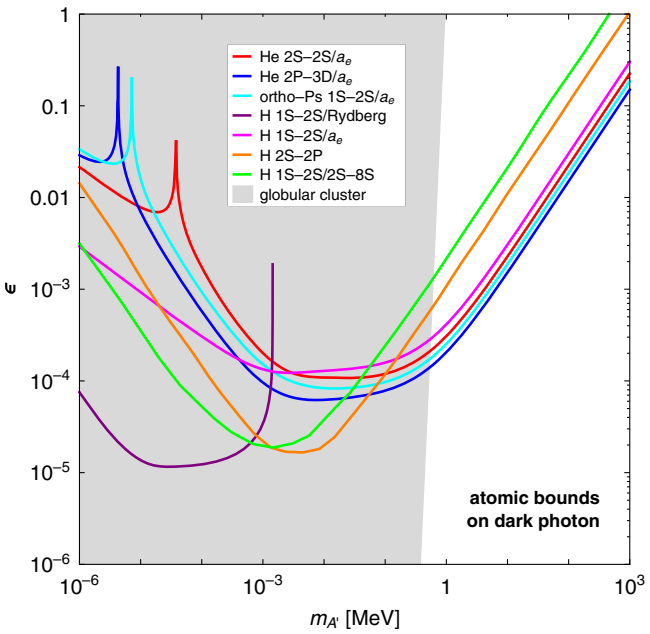

FIG. 6. Comparison of atomic (indirect) constraints on the mixing ϵ between the photon and the dark photon A' depending on its mass $m_{A'}$. The red/blue (cyan) lines refer to He (positronium) transitions obtained in this work. For comparison, previous bounds from H spectroscopy are shown for $1S-2S$ combined with Rydberg states (purple) or a_e (pink) [23,24,93] and from one or the combination of two H transitions (orange, green) [25]. The range of $m_{A'} \leq 300$ keV is excluded by globular clusters [45]; for $m_{A'} \gtrsim 1$ MeV several direct, decay-dependent bounds also apply.

bounds surpass the known hydrogen bounds above ~100 keV. We chose to present only indirect constraints from atomic spectroscopy on the kinetic-mixing parameter since those do not depend on the A' decay mode. In the sub-MeV region, these atomic probes are the most sensitive ones, after the LSND neutrino detector which directly searches for A' in the 3 photons decay [92], and the study of star cooling in globular clusters which excludes, for $m_{A'} \lesssim 300$ keV, mixing parameter values far below the displayed range of ϵ in Fig. 6. For $m_{A'} \gtrsim 1$ MeV, the sensitivity of atomic spectroscopy is also much weaker compared to probes based on A' decay (either visibly or invisibly) as in electron beam-dump experiments or colliders, like *BABAR* (see Ref. [62] for a review). In conclusion, for $m_{A'} \gtrsim 0.3$ MeV, the most sensitive indirect probe of dark photon is from combining a_e with atomic transitions in helium.

V. DISCUSSION

In this work we study the sensitivity to new spin-independent forces of hydrogen and heliumlike atoms considering both absolute frequency and isotope shift measurements. We exploit the accuracy of both the measurements and the theoretical predictions achieved in these systems [21,22]. We demonstrate for the first time the power of isotope shift measurements in few-electrons atoms to constrain models where the new degree of freedom, ϕ, couples not only to the proton, but also to the neutron as, for instance, in the $B-L$ and Higgs portal models. The derived bounds represent, to date, the strongest laboratory bound on $y_e y_n$ for $m_\phi \gtrsim 100$ eV. For masses heavier than 300 keV, where astrophysical probes are ineffective, isotope shift spectroscopy in few-electron atoms constrains new regions of the parameter space in a model-independent way. Previous works on spin-independent new interactions [23–25] focused on hydrogen which is only sensitive to new interactions between the electron and the proton. The highly precise spectroscopy of helium has the advantage to probe also the electron coupling alone, reaching a sensitivity comparable to a_e below few keV. (See Ref. [26] for similar results regarding spin-dependent electron-electron interactions.) Furthermore, we show that current precision in positronium spectroscopy has comparable constraining power.

The present work emphasizes how the effort in improving the knowledge of the nuclear size has the indirect effect of improving the sensitivity to new spin-independent forces between the constituents of the atoms.

TABLE II. Charge radii r_A used for the IS bounds for different elements with isotopes A, obtained via electron-scattering experiments (e-scat.) or spectroscopy in muonic atoms (μ-spec.).

Element	A	r_A [fm]	Method	Reference
H/D	1	0.8791 ± 0.0079	e-scat.	[94]
	2	2.130 ± 0.010		[94]
	1	0.84087 ± 0.00039	μ-spec.	[34,35]
	2	2.12562 ± 0.00078		[36]
He	3	1.973 ± 0.016	e-scat.	[72]
	4	1.681 ± 0.004		[72]
Li	6	2.589 ± 0.039	e-scat.	[95]
	7	2.444 ± 0.042		
N	14	2.560 ± 0.011	μ-spec.	[80]
	15	2.612 ± 0.009	e-scat.	[79]

ACKNOWLEDGMENTS

We thank D. Budker, R. Ozeri, K. Pachucki and G. Perez for useful discussions and careful reading of the manuscript. We thank G. Bélanger, J. Berengut, A. Falkowski, O. Hen, J. Jaeckel, R. P. M. J. W. Notermans and M. Safranova for useful discussions and correspondence. C. D. is supported by the program Initiative d'Excellence of Grenoble-Alpes University under grant Contract No. ANR-15-IDEX-02. The work of Y. S. is supported by the Office of High Energy Physics of U.S. Department of Energy (DOE) under grant Contract No. DE-SC0012567.

APPENDIX A: EXPERIMENTAL DATA AND THEORETICAL PREDICTION

In this appendix we provide all experimental data and theoretical predictions that have been used in this paper.

We start with the nuclear charge radii in Table II used throughout the paper.

TABLE III. Theoretical and experimental input values for the IS bounds: measured IS $\nu_i^{AA',\mathrm{exp}}$, theory prediction for a point-like nucleus $\nu_{i,0}^{AA',\mathrm{th}}$, and the field shift constant F_i. See also Ref. [21]. For the IS of $2S-12D$ in H/D, see the absolute frequencies in Table IV. F_{1S-2S} for H/D is an approximate value obtained from the quoted FS in Ref. [82].

A, A'	Transition i	$\nu_i^{AA',\mathrm{exp}}$ [kHz]	Reference	$\nu_{i,0}^{AA',\mathrm{th}}$ [kHz]	F_i [kHz/fm^2]	Reference
^{3,4}He	$2^1S_0-2^3S_1$	$-8\,034\,286.259 \pm 2.4$	[96–98]	$-8\,034\,065.91 \pm 0.19$	-214.66 ± 0.02	[30,99–101]
	$2^3P-2^3S_1$	$-33\,668\,444.7 \pm 3.2$		$-33\,667\,149.3 \pm 0.9$	$-1\,212.2 \pm 0.1$	
^{4,8}He	$2^3S_1-3^3P_2$	$64\,701\,466 \pm 52$	[102]	64 702 409	1 008	[102]
H/D	$1S-2S$	$670\,994\,334.605 \pm 0.015$	[82]	$670\,999\,566.90 \pm 0.89$	$-1\,369.88$	[82]
^{14,15}N	$2^1S_0-2^3P_1$	$649\,418\,424.16 \pm 29\,979.2$	[77]	$649\,469\,388.8 \pm 269\,812.8$		[77]
^{6,7}Li	$2^3P_0-2^3S_1$	$3\,474\,773 \pm 55$	[76]	34 747 876		[76]

TABLE IV. Measurements and predictions of absolute transition frequencies in H, D, He and positronium (Ps). The H and D values are used for the H/D IS in Sec. III B. The middle part of the table summarizes the experimental and theoretical frequencies of the Lamb shift $(4L-2S_{1/2})-\frac{1}{4}(2S-1S)$ for $L=S, D$. The lower part of the table is used for constraining y_e in Fig. 4: the transitions in ^{4}He with an agreement of better than 2σ between theory and experiment, as well as a transition in Ps.

Element	Transition i	$\nu_i^{\rm exp}$ [kHz]	Reference	$\nu_i^{\rm th}$ [kHz]	Reference
H	$2S_{1/2}-12D_{3/2,5/2}$	$799\,191\,727\,402.8 \pm 6.7$	[83]	$799\,191\,727\,409.1 \pm 3.0$	[103]
D		$799\,409\,184\,967.6 \pm 6.5$		$799\,409\,184\,973.4 \pm 3.0$	
H	$(4S_{1/2}-2S_{1/2})-\frac{1}{4}(2S-1S)$	4797338 ± 10	[86]	$4\,797\,329 \pm 5$	[86]
D		$4\,801\,693 \pm 20$		$4\,801\,692 \pm 5$	
H	$(4S_{1/2}-2D_{5/2})-\frac{1}{4}(2S-1S)$	$6\,490\,144 \pm 24$		$6\,490\,128 \pm 5$	
D		$6\,494\,841 \pm 41$		$6\,494\,816 \pm 5$	
^{4}He	$2^1S_0-2^3S_1$	$192\,510\,702\,145.6 \pm 1.8$	[69]	$192\,510\,703\,400 \pm 800$	[21]
	$2^3P_0-3^3D_1$	$510\,059\,755\,352 \pm 28$	[104]	$510\,059\,754\,000 \pm 700$	
	$2^3S_1-3^3D_1$	$786\,823\,850\,002 \pm 56$	[105]	$786\,823\,848\,400 \pm 1\,300$	
	$2^1S_0-2^1P_1$	$145\,622\,892\,886 \pm 183$	[106]	$145\,622\,891\,500 \pm 2\,300$	
	$2^3P-2^3S_1$	$276\,736\,495\,649 \pm 2$	[71]	$276\,736\,495\,400 \pm 2\,000$	
	$2^3S_1-2^1P_1$	$338\,133\,594\,400 \pm 500$	[107]	$338\,133\,594.900 \pm 1\,400$	
Ps	$1^3S_1-2^3S_1$	$1\,233\,607\,216\,400 \pm 3200$	[89]	$1\,233\,607\,222\,180 \pm 580$	[90]

In Table III we continue with the input values used for the IS bounds in Table I and Fig. 2 of Sec. III, see also Table 5 of Ref. [21]. Finally, we provide the values of measurements and calculations of absolute frequencies in Table IV.

APPENDIX B: HELIUM WAVE FUNCTION

In this appendix we specify the approximate wave functions we use in the helium calculations. It is conventional to label the states of helium as

$$n^{2S+1}L_J \tag{B1}$$

corresponding to the following electronic configuration $(1s)(nl)$. L is the total orbital momentum, S is the spin and $J \le L+S$ is the total angular momentum. Since one electron is always in the $(1s)$ orbital $L=l$, and $S=0, 1$ corresponding to the singlet and triplet states, respectively.

For two-electron systems in the nonrelativistic limit, the spin and spatial parts of the wave function are factorized. The spin singlet ($S=0$) state is

$$|S=0, m_S=0\rangle = \frac{|\uparrow\downarrow\rangle - |\downarrow\uparrow\rangle}{\sqrt{2}}, \tag{B2}$$

while the spin triplet ($S=1$) is with components

$$\begin{aligned} |S=1, m_S=1\rangle &= |\uparrow\uparrow\rangle, \\ |S=1, m_S=0\rangle &= \frac{|\uparrow\downarrow\rangle + |\downarrow\uparrow\rangle}{\sqrt{2}}, \\ |S=1, m_S=-1\rangle &= |\downarrow\downarrow\rangle. \end{aligned} \tag{B3}$$

Using an antisymmetrized combination of hydrogenic orbitals, the spatial part of the wave function takes the form

$$\begin{aligned} &\langle \vec{r}_1, \vec{r}_2 | \psi^S_{nlm}\rangle \\ &\quad = \frac{1}{2\sqrt{\pi}} \frac{1}{\sqrt{2(1+N_{nl})}} \\ &\qquad \times [F_{nl}(r_1, r_2) Y_{lm}(\Omega_2) + (-1)^S F_{nl}(r_2, r_1) Y_{lm}(\Omega_1)], \end{aligned} \tag{B4}$$

where the $1/(2\sqrt{\pi})$ prefactor is the Y_{00} spherical harmonic from the $1s$ electron, and N_{nl} ensures that the radial part of the wave function is canonically normalized. We write the F_{nl}'s as products of nonrelativistic hydrogen radial wave functions as

$$F_{nl}(r_1, r_2) = R_{10}(r_1, Z_i) R_{nl}(r_2, Z_a), \tag{B5}$$

where (in units of $a_0 = 1$)

$$R_{nl}(r, Z) = \left(\frac{2Z}{n}\right)^{3/2} \sqrt{\frac{(n-l-1)!}{2n(n+l)!}} e^{-\rho/2} \rho^l L^{2l+1}_{n-l-1}(\rho), \tag{B6}$$

where $\rho = 2rZ/n$, $L^\alpha_k(x)$ are the generalized Laguerre polynomials of degree k, and Z_i and Z_a are the effective nuclear charges for the core $(1s)$ and valence (nl) electrons, respectively. An important point is that $Z_{i,a} \neq Z = 2$ because of screening effects; they depend on the electronic configuration considered, see Table V. The R_{nl}'s form an orthonormal basis for a fixed Z. However, because the two electrons effectively feel a different nuclear charge ($Z_i \neq Z_a$), there is an overall normalization constant for S waves because of the cross term in the square of Eq. (B4)

$$N_{nl} = (-1)^S \delta_{l,0} \left[\int dr r^2 R_{10}(r, Z_i) R_{nl}(r, Z_a)\right]^2, \tag{B7}$$

which vanishes for $Z_i = Z_a$ and $n \ge 2$ by orthogonality of $R_{nl}(r, Z)$.

TABLE V. Effective nuclear charges for the excited states of helium under consideration. Z_i is the charge of the core $(1s)$ electron and Z_a is the charge of the excited electron. These are obtained by variational methods using the nonrelativistic hydrogen wave functions as trial functions. When the electron is excited to a $n = 3$ or higher orbital, the screening of the core electron is found nearly perfect.

State	Z_i	Z_a
$(2)^1S$	2.08	1.21
$(2)^3S$	2.01	1.53
$(2)^3P$	2.00	0.97
$(2)^3P$	1.99	1.09
$n \geq 3$	2	1

The total wave function for a fixed J and (its projection) $m_J = -J \ldots J$ are then constructed from $L \times S$ combination of angular momentum using the Clebsch-Gordan coefficients C^{J,m_J}_{L,m,S,m_S} as

$$|n^{2S+1}L_{J,m_J}\rangle = \sum_{m=-L}^{L} \sum_{m_S=-S}^{S} C^{J,m_J}_{L,m,S,m_S} |\psi_{nLm}\rangle |S, m_S\rangle. \quad \text{(B8)}$$

We use the above wave functions for all helium states with the exceptions of the 2^1S, 2^3S and 2^3P states where we use non-relativistic wave functions based on Hylleraas functions taken from Refs. [108,109] in order to better describe the repulsion between the two electrons. This turns out to be of particular importance for the 2^1S state. Indeed, for spin-singlet states, the spatial part of the wave function is symmetric under the exchange of the two-electrons so that the wave function in Eq. (B4) may overestimate the electronic density is in the region where the electrons are close to each other, $r_1 \sim r_2$. Hylleraas functions then provide a more accurate description of the electron repulsion effect by introducing an explicit dependence on the interelectronic distance r_{12} in the wave function. The spatial part of wave function is then taken to be of the form

$$\langle \vec{r}_1, \vec{r}_2 | \psi^S_{nlm} \rangle = \frac{1}{\sqrt{N}} [F_{nl}(r_1, r_2, r_{12}) Y_{lm}(\Omega_2) + (-1)^S F_{nl}(r_2, r_1, r_{12}) Y_{lm}(\Omega_1)] \quad \text{(B9)}$$

where N is a normalization constant and F_{nl} now depends on r_{12} and is expanded on Hylleraas functions as

$$F_{nl}(r_1, r_2, r_{12}) = [\kappa(s+t)]^l e^{-\frac{\kappa}{2}(s-\sigma t)} \sum_{i=1}^{k} c_i \phi_i(\kappa s, -\kappa t, \kappa u), \quad \text{(B10)}$$

with $s \equiv r_1 + r_2$, $t \equiv r_2 - r_1$, $u \equiv r_{12}$ and $\phi_i(s,t,u) = s^{p_i} t^{q_i} u^{r_i}$. It is convenient to reorganize the Hylleraas terms according to their powers of r_{12}. We then write the radial function in Eq. (B10) as

$$F_{nl}(r_1, r_2, r_{12}) = \sum_{i=0}^{k} f_i(r_1, r_2) r^i_{12}. \quad \text{(B11)}$$

APPENDIX C: OVERLAP INTEGRALS FOR HELIUM

In this appendix we give the analytical expressions for the overlap integrals for the case of helium, i.e. the electronic NP coefficients X_i and Y_i.

1. Electron-nucleus interactions

Let us consider the potential of Eq. (1) between the nucleus and its bound electron with the above helium wave functions. In first-order perturbation theory we find

$$X_i \equiv \hat{X}_a - \hat{X}_b = \frac{1}{4\pi} \int \left[\prod_{k=1}^{n_e} d^3 r_k\right] \left[\sum_{k=1}^{n_e} \frac{e^{-m_\phi r_k}}{r_k}\right] \times [|\Psi_a(\vec{r}_1, \ldots, \vec{r}_{n_e})|^2 - |\Psi_b(\vec{r}_1, \ldots, \vec{r}_{n_e})|^2], \quad \text{(C1)}$$

where n_e is the number of bound electrons and $|\Psi|^2$ is the electron wave function density. Using hydrogenic wave functions in Eq. (B4) the contributions from each state is

$$\hat{X}_{n^{2S+1}L_{J,m_J}} = -\frac{1}{4\pi(1+N_{nL})} \left[\int dr r e^{-m_\phi r} [R_{10}(r, Z_i)^2 + R_{nL}(r, Z_a)^2] + 2(-1)^S \delta_{L,0} \int dr r e^{-m_\phi r} R_{10}(r, Z_i) R_{nL}(r, Z_a) \int dr r^2 R_{10}(r, Z_i) R_{nL}(r, Z_a)\right]. \quad \text{(C2)}$$

For the case of Hylleraas wave functions in Eq. (B9), we need the following expansion of r_{12} raised to the power k on spherical harmonics

$$r^k_{12} = 4\pi \sum_{l=0}^{\infty} H^{(k)}_l(r_1, r_2) \sum_{m=-l}^{l} Y_{lm}(\Omega_1) Y^*_{lm}(\Omega_2), \quad \text{(C3)}$$

where the coefficients can be written in closed form in terms of hypergeometric functions [110]

$$H_l^{(n)}(r_1,r_2) = \frac{(-n/2)_l}{(1/2)_l}\frac{r_>^n}{2l+1}\left(\frac{r_<}{r_>}\right)^l \times F\left[l-n/2,-(n+1)/2;l+3/2;\frac{r_<^2}{r_>^2}\right], \tag{C4}$$

with $F(\alpha,\beta;\gamma;x)$ denoting the Gauss hypergeometric function and $(\xi)_s \equiv \Gamma(\xi+s)/\Gamma(\xi)$. We then find

$$\hat{X}_{n^{2S+1}L_{J,m_J}} = -\frac{1}{4\pi N}\int r_1^2 r_2^2 dr_1 dr_2\left(\frac{e^{-m_\phi r_1}}{r_1}+\frac{e^{-m_\phi r_2}}{r_2}\right) \times \int d\Omega_1 d\Omega_2 |\psi^S_{nlm}|^2, \tag{C5}$$

where the square of the spatial wave function integrated over the angular variables is

$$\begin{aligned}\int d\Omega_1 d\Omega_2 |\psi^S_{nlm}|^2 &= f_0(r_1,r_2)^2 + \sum_{i+j\geq 1} H_0^{(i+j)}(r_1,r_2) f_i(r_1,r_2) f_j(r_1,r_2) \\ &+ [r_1 \leftrightarrow r_2] + 2(-1)^S\Big[f_0(r_1,r_2)f_0(r_2,r_1)\delta_{l0} \\ &+ \sum_{i+j\geq 1} H_l^{(i+j)}(r_1,r_2) f_i(r_1,r_2) f_j(r_2,r_1)\Big].\end{aligned} \tag{C6}$$

2. Electron-electron interactions

Consider the NP potential between the bounded electrons, $V_e(r_{12})$ see Eq. (1). It is useful to expand the Yukawa potential over spherical harmonics as, see for example [111],

$$\frac{e^{-mr_{12}}}{r_{12}} = 4\pi\sum_{l=0}^{\infty} G_l(r_1,r_2,m)\sum_{m=-l}^{l} Y_{lm}(\Omega_1)Y^*_{lm}(\Omega_2), \tag{C7}$$

where the coefficients are

$$G_l(r_1,r_2,m) = \frac{I_{l+1/2}(mr_<)}{\sqrt{r_<}}\frac{K_{l+1/2}(mr_>)}{\sqrt{r_>}}, \tag{C8}$$

with I and K the modified Bessel functions of the first and second kind respectively and $r_>$ ($r_<$) is the greater (lesser) of r_1 and r_2. For Hylleraas wave functions which involve additional powers of r_{12} it will be convenient to use Eq. (C7) as a "generating functional" in order to derive the expansion of any $r_{12}^{k-1}e^{-mr_{12}}$ functions (for $k \geq 1$) by differentiating k-times the coefficients $G_l(r_1,r_2,m)$.

The first-order perturbation theory result is

$$\begin{aligned}Y_i &\equiv \hat{Y}_a - \hat{Y}_b \\ &= \frac{1}{4\pi}\int\left[\prod_{k=1}^{n_e} d^3 r_k\right]\left[\sum_{i>j}^{n_e}\frac{e^{-m_\phi r_{ij}}}{r_{ij}}\right] \\ &\times [|\Psi_a(\overrightarrow{r_1},\ldots,\overrightarrow{r_{n_e}})|^2 - |\Psi_b(\overrightarrow{r_1},\ldots,\overrightarrow{r_{n_e}})|^2].\end{aligned} \tag{C9}$$

Using the expansion of Eq. (C7) and the hydrogenic wave functions from Eq. (B4) we find

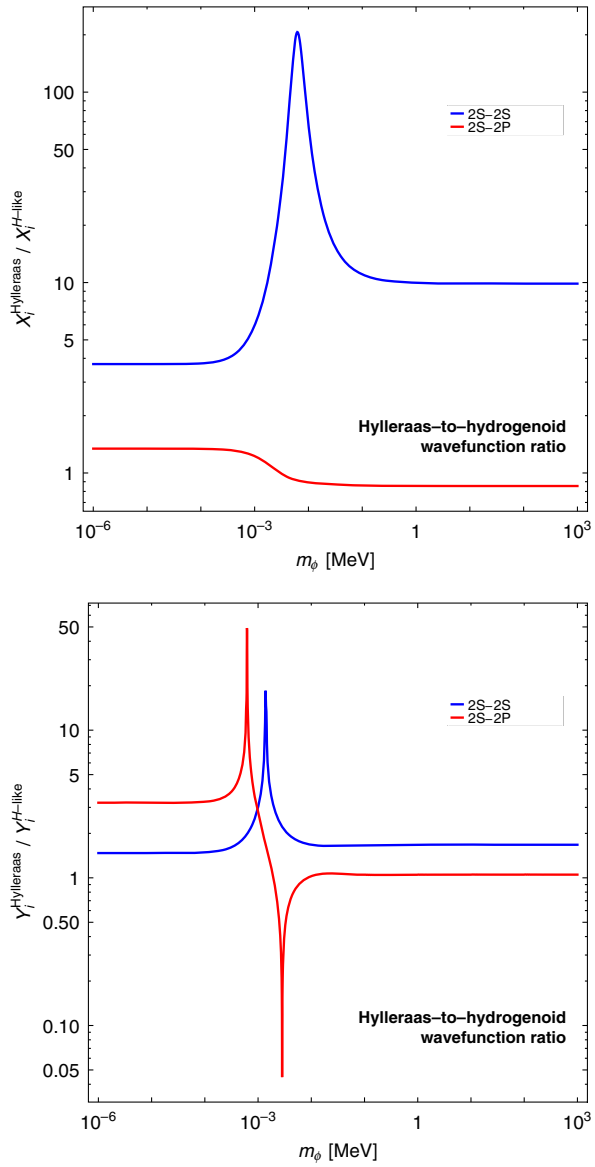

FIG. 7. Comparison of the electronic NP coefficients X_i, Y_i based on hydrogen-like and Hylleraas wave functions depending on the mediator mass m_ϕ for the transitions $2S-2S$ and $2P-2S$ in helium.

$$\hat{Y}_{n^{2S+1}L_{J,m_J}} = -\frac{1}{4\pi(1+N_{nL})}\int dr_1 dr_2 r_1^2 r_2^2 [G_0(r_1,r_2)R_{10}(r_1,Z_i)^2 R_{nL}(r_2,Z_a)^2 + (-1)^S G_L(r_1,r_2)R_{10}(r_1,Z_i)R_{10}(r_2,Z_i)R_{nL}(r_1,Z_a)R_{nL}(r_2,Z_a)]. \quad \text{(C10)}$$

where only $G_{0,L}$ coefficients in the Yukawa expansion of Eq. (C7) are needed. Note that the integrand above no longer depends on m' and m_S hence the sum over Clebsch-Gordan coefficients squared gives $\sum_{m',m_S}[C^{J,m_J}_{L,m',S,m_S}]^2 = 1$ by orthonormality. Finally, note that the shift in Eq. (C10) is independent of J and m_J, which is expected since the potential in Eq. (1) is invariant under rotations. We also used the fact the $G_l(r_1,r_2) = G_l(r_2,r_1)$ to simplify the expression.

For the case of Hylleraas wave functions in Eq. (B9), we find

$$\hat{Y}_{n^{2S+1}L_{J,m_J}} = -\frac{1}{4\pi N}\int r_1^2 r_2^2 dr_1 dr_2 \times \int d\Omega_1 d\Omega_2 \frac{e^{-mr_{12}}}{r_{12}}|\psi^S_{nlm}|^2, \quad \text{(C11)}$$

where the angular integral simplifies to

$$\int d\Omega_1 d\Omega_2 \frac{e^{-mr_{12}}}{r_{12}}|\psi^S_{nlm}|^2 = \sum_{ij} G_0^{(i+j)}(r_1,r_2)[f_i(r_1,r_2)f_j(r_1,r_2)+f_i(r_2,r_1)f_j(r_2,r_1)] + 2(-1)^S \sum_{ij} G_l^{(i+j)}(r_1,r_2)f_i(r_1,r_2)f_j(r_2,r_1), \quad \text{(C12)}$$

where $^{(k)}$ indicates the kth differentiation with respect to m,

$$G_l^{(k)}(r_1,r_2,m) \equiv (-1)^k \frac{\partial^k G_l(r_1,r_2,m)}{\partial m^k}. \quad \text{(C13)}$$

In Fig. 7 we evaluate the impact of the Hylleraas wave functions on the electronic NP constants by calculating the ratios to the respective quantity based on hydrogen-like wave functions, $X_i^{\text{Hylleraas}}/X_i^{\text{H-like}}$, $Y_i^{\text{Hylleraas}}/Y_i^{\text{H-like}}$.

[1] S. G. Porsev, K. Beloy, and A. Derevianko, Precision Determination of Electroweak Coupling from Atomic Parity Violation and Implications for Particle Physics, Phys. Rev. Lett. **102**, 181601 (2009).

[2] K. Tsigutkin, D. Dounas-Frazer, A. Family, J. E. Stalnaker, V. V. Yashchuk, and D. Budker, Observation of a Large Atomic Parity Violation Effect in Ytterbium, Phys. Rev. Lett. **103**, 071601 (2009).

[3] K. Tsigutkin, D. Dounas-Frazer, A. Family, J. E. Stalnaker, V. V. Yashchuk, and D. Budker, Parity violation in atomic ytterbium: Experimental sensitivity and systematics, Phys. Rev. A **81**, 032114 (2010).

[4] N. Leefer, L. Bougas, D. Antypas, and D. Budker, Towards a new measurement of parity violation in dysprosium, arXiv:1412.1245.

[5] O. O. Versolato *et al.*, Atomic parity violation in a single trapped radium ion, Hyperfine Interact. **199**, 9 (2011).

[6] V. A. Dzuba, J. C. Berengut, V. V. Flambaum, and B. Roberts, Revisiting Parity Non-conservation in Cesium, Phys. Rev. Lett. **109**, 203003 (2012).

[7] B. M. Roberts, V. A. Dzuba, and V. V. Flambaum, Parity and time-reversal violation in atomic systems, Annu. Rev. Nucl. Part. Sci. **65**, 63 (2015).

[8] K. P. Jungmann, Symmetries and fundamental interactions-selected topics, Hyperfine Interact. **227**, 5 (2014).

[9] K. A. Olive *et al.* (Particle Data Group Collaboration), Review of particle physics, Chin. Phys. C **38**, 090001 (2014).

[10] R. M. Godun, P. B. R. Nisbet-Jones, J. M. Jones, S. A. King, L. A. M. Johnson, H. S. Margolis, K. Szymaniec, S. N. Lea, K. Bongs, and P. Gill, Frequency Ratio of Two Optical Clock Transitions in $^{171}Yb^+$ and Constraints on the Time Variation of Fundamental Constants, Phys. Rev. Lett. **113**, 210801 (2014).

[11] N. Huntemann, M. Okhapkin, B. Lipphardt, S. Weyers, C. Tamm, and E. Peik, High-Accuracy Optical Clock Based on the Octupole Transition in $^{171}Yb^+$, Phys. Rev. Lett. **108**, 090801 (2012).

[12] J. Reichert, M. Niering, R. Holzwarth, M. Weitz, T. Udem, and T. W. Hänsch, Phase Coherent Vacuum-Ultraviolet to Radio Frequency Comparison with a Mode-Locked Laser, Phys. Rev. Lett. **84**, 3232 (2000).

[13] J. Reichert, R. Holzwarth, T. Udem, and T. Hänsch, Measuring the frequency of light with mode-locked lasers, Opt. Commun. **172**, 59 (1999).

[14] N. Huntemann, C. Sanner, B. Lipphardt, C. Tamm, and E. Peik, Single-Ion Atomic Clock with 3×10^{-18} Systematic Uncertainty, Phys. Rev. Lett. **116**, 063001 (2016).

[15] B. J. Bloom, T. L. Nicholson, J. R. Williams, S. L. Campbell, M. Bishof, X. Zhang, W. Zhang, S. L. Bromley, and J. Ye,

An optical lattice clock with accuracy and stability at the 10^{-18} level, Nature (London) **506**, 71 (2014).
[16] C. Delaunay, R. Ozeri, G. Perez, and Y. Soreq, Probing the atomic Higgs force, Phys. Rev. D **96**, 093001 (2017).
[17] C. Frugiuele, E. Fuchs, G. Perez, and M. Schlaffer, Constraining new physics models with isotope shift spectroscopy, Phys. Rev. D **96**, 015011 (2017).
[18] C. Delaunay and Y. Soreq, Probing new physics with isotope shift spectroscopy, arXiv:1602.04838.
[19] J. C. Berengut *et al.*, Probing new light force-mediators by isotope shift spectroscopy, arXiv:1704.05068.
[20] W. H. King, Comments on the article, Peculiarities of the isotope shift in the Samarium spectrum, J. Opt. Soc. Am. **53**, 638 (1963).
[21] K. Pachucki, V. Patkóš, and V. Yerokhin, Testing fundamental interactions on the helium atom, Phys. Rev. A **95**, 062510 (2017).
[22] S. G. Karshenboim, Precise physics of simple atoms, AIP Conf. Proc. **551**, 238 (2001).
[23] S. G. Karshenboim, Constraints on a long-range spin-independent interaction from precision atomic physics, Phys. Rev. D **82**, 073003 (2010).
[24] S. G. Karshenboim, Precision Physics of Simple Atoms and Constraints on a Light Boson with Ultraweak Coupling, Phys. Rev. Lett. **104**, 220406 (2010).
[25] J. Jaeckel and S. Roy, Spectroscopy as a test of Coulomb's law: A probe of the hidden sector, Phys. Rev. D **82**, 125020 (2010).
[26] F. Ficek, D. F. J. Kimball, M. Kozlov, N. Leefer, S. Pustelny, and D. Budker, Constraints on exotic spin-dependent interactions between electrons from helium fine-structure spectroscopy, Phys. Rev. A **95**, 032505 (2017).
[27] C. Eckart, The theory, and calculation of screening constants, Phys. Rev. **36**, 878 (1930).
[28] E. A. Hylleraas, Über den grundzustand des heliumatoms, Z. Phys. **48**, 469 (1928).
[29] E. A. Hylleraas, Neue berechnung der energie des heliums im grundzustande, sowie des tiefsten terms von orthohelium, Z. Phys. **54**, 347 (1929).
[30] K. Pachucki and V. A. Yerokhin, Theory of the helium isotope shift, J. Phys. Chem. Ref. Data **44**, 031206 (2015).
[31] Y.-S. Liu, D. McKeen, and G. A. Miller, Electrophobic Scalar Boson and Muonic Puzzles, Phys. Rev. Lett. **117**, 101801 (2016).
[32] D. Tucker-Smith and I. Yavin, Muonic hydrogen and MeV forces, Phys. Rev. D **83**, 101702 (2011).
[33] I. Beltrami *et al.*, New precision measurements of the muonic 3-D $(5/2)$-$2p(3/2)$ x-ray transition in ^{24}Mg and ^{28}Si: Vacuum polarization test and search for muon-hadron interactions beyond QED, Nucl. Phys. **A451**, 679 (1986).
[34] R. Pohl *et al.*, The size of the proton, Nature (London) **466**, 213 (2010).
[35] A. Antognini *et al.*, Proton structure from the measurement of $2S-2P$ transition frequencies of muonic hydrogen, Science **339**, 417 (2013).
[36] R. Pohl *et al.* (CREMA Collaboration), Laser spectroscopy of muonic deuterium, Science **353**, 669 (2016).
[37] F. Gebert, Y. Wan, F. Wolf, C. N. Angstmann, J. C. Berengut, and P. O. Schmidt, Precision Isotope Shift Measurements in Calcium Ions Using Quantum Logic Detection Schemes, Phys. Rev. Lett. **115**, 053003 (2015).
[38] M. Bordag, U. Mohideen, and V. M. Mostepanenko, New developments in the Casimir effect, Phys. Rep. **353**, 1 (2001).
[39] M. Bordag, G. L. Klimchitskaya, U. Mohideen, and V. M. Mostepanenko, Advances in the Casimir effect, Int. Ser. Monogr. Phys. **145**, 1 (2009).
[40] S. L. Adler, R. F. Dashen, and S. B. Treiman, Comments on proposed explanations for the mu-mesic atom x-ray discrepancy, Phys. Rev. D **10**, 3728 (1974).
[41] R. Barbieri and T. E. O. Ericson, Evidence against the existence of a low mass scalar boson from neutron-nucleus scattering, Phys. Lett. **57B**, 270 (1975).
[42] H. Leeb and J. Schmiedmayer, Constraint on Hypothetical Light Interacting Bosons from Low-Energy Neutron Experiments, Phys. Rev. Lett. **68**, 1472 (1992).
[43] V. V. Nesvizhevsky, G. Pignol, and K. V. Protasov, Neutron scattering and extra short range interactions, Phys. Rev. D **77**, 034020 (2008).
[44] Yu. N. Pokotilovski, Constraints on new interactions from neutron scattering experiments, Phys. At. Nucl. **69**, 924 (2006).
[45] E. Hardy and R. Lasenby, Stellar cooling bounds on new light particles: Plasma mixing effects, J. High Energy Phys. 02 (2017) 033.
[46] C. Patrignani *et al.* (Particle Data Group Collaboration), Review of particle physics, Chin. Phys. C **40**, 100001 (2016).
[47] D. Hanneke, S. F. Hoogerheide, and G. Gabrielse, Cavity control of a single-electron quantum cyclotron: Measuring the electron magnetic moment, Phys. Rev. A **83**, 052122 (2011).
[48] G. Raffelt, Limits on a CP-violating scalar axion-nucleon interaction, Phys. Rev. D **86**, 015001 (2012).
[49] W. M. Yao *et al.* (Particle Data Group Collaboration), Review of particle physics, J. Phys. G **33**, 1 (2006).
[50] J. A. Grifols and E. Masso, Constraints on finite range baryonic and leptonic forces from stellar evolution, Phys. Lett. **173B**, 237 (1986).
[51] J. A. Grifols, E. Masso, and S. Peris, Energy lLoss from the sun and RED giants: Bounds on short range baryonic and leptonic forces, Mod. Phys. Lett. A **04**, 311 (1989).
[52] J. Redondo and G. Raffelt, Solar constraints on hidden photons re-visited, J. Cosmol. Astropart. Phys. 08 (2013) 034.
[53] E. J. Salumbides, W. Ubachs, and V. I. Korobov, Bounds on fifth forces at the sub-Angstrom length scale, J. Mol. Spectrosc. **300**, 65 (2014).
[54] W. Ubachs, J. C. J. Koelemeij, K. S. E. Eikema, and E. J. Salumbides, Physics beyond the standard model from hydrogen spectroscopy, arXiv:1511.00985.
[55] J. Biesheuvel, J.-P. Karr, L. Hilico, K. S. E. Eikema, W. Ubachs, and J. C. J. Koelemeij, High-precision spectroscopy of the HD+molecule at the 1-p.p.b. level, Appl. Phys. B **123**, 23 (2017).
[56] W. Ubachs, J. C. J. Koelemeij, K. S. E. Eikema, and E. J. Salumbides, Physics beyond the standard model from hydrogen spectroscopy, J. Mol. Spectrosc. **320**, 1 (2016).

[57] B. Feldman and A. E. Nelson, New regions for a chameleon to hide, J. High Energy Phys. 08 (2006) 002.
[58] A. E. Nelson and J. Walsh, Chameleon vector bosons, Phys. Rev. D **77**, 095006 (2008).
[59] C. Burrage, Supernova brightening from chameleon-photon mixing, Phys. Rev. D **77**, 043009 (2008).
[60] C. Burrage and J. Sakstein, A compendium of chameleon constraints, J. Cosmol. Astropart. Phys. 11 (2016) 045.
[61] P. Brax and C. Burrage, Atomic precision tests and light scalar couplings, Phys. Rev. D **83**, 035020 (2011).
[62] J. Alexander *et al.*, Dark sectors 2016 workshop: Community report, arXiv:1608.08632.
[63] N. Leefer, A. Gerhardus, D. Budker, V. V. Flambaum, and Y. V. Stadnik, Search for the Effect of Massive Bodies on Atomic Spectra and Constraints on Yukawa-Type Interactions of Scalar Particles, Phys. Rev. Lett. **117**, 271601 (2016).
[64] L. Zhou, S. Long, B. Tang, X. Chen, F. Gao, W. Peng, W. Duan, J. Zhong, Z. Xiong, J. Wang, Y. Zhang, and M. Zhan, Test of Equivalence Principle at 10^{-8} Level by a Dual-Species Double-Diffraction Raman Atom Interferometer, Phys. Rev. Lett. **115**, 013004 (2015).
[65] M. G. Tarallo, T. Mazzoni, N. Poli, D. V. Sutyrin, X. Zhang, and G. M. Tino, Test of Einstein Equivalence Principle for 0-Spin and Half-Integer-Spin Atoms: Search for Spin-Gravity Coupling Effects, Phys. Rev. Lett. **113**, 023005 (2014).
[66] D. Schlippert, J. Hartwig, H. Albers, L. L. Richardson, C. Schubert, A. Roura, W. P. Schleich, W. Ertmer, and E. M. Rasel, Quantum Test of the Universality of Free Fall, Phys. Rev. Lett. **112**, 203002 (2014).
[67] A. Bonnin, N. Zahzam, Y. Bidel, and A. Bresson, Simultaneous dual-species matter-wave accelerometer, Phys. Rev. A **88**, 043615 (2013).
[68] S. Fray, C. A. Diez, T. W. Hänsch, and M. Weitz, Atomic Interferometer with Amplitude Gratings of Light and Its Applications to Atom Based Tests of the Equivalence Principle, Phys. Rev. Lett. **93**, 240404 (2004).
[69] R. van Rooij, J. S. Borbely, J. Simonet, M. D. Hoogerland, K. S. E. Eikema, R. A. Rozendaal, and W. Vassen, Frequency metrology in quantum degenerate helium: Direct measurement of the $2^3S_1 \rightarrow 2^1S_0$ transition, Science **333**, 196 (2011).
[70] P. C. Pastor, L. Consolino, G. Giusfredi, P. De Natale, M. Inguscio, V. A. Yerokhin, and K. Pachucki, Frequency Metrology of Helium around 1083 nm and Determination of the Nuclear Charge Radius, Phys. Rev. Lett. **108**, 143001 (2012).
[71] P. C. Pastor, G. Giusfredi, P. D. Natale, G. Hagel, C. de Mauro, and M. Inguscio, Absolute Frequency Measurements of the $2^3S_1 \rightarrow 2^3P_{0,1,2}$ Atomic Helium Transitions around 1083 nm, Phys. Rev. Lett. **92**, 023001 (2004).
[72] I. Sick, Form factors, and radii of light nuclei, arXiv:1505.06924.
[73] A. Antognini *et al.*, Illuminating the proton radius conundrum: The mu He + Lamb shift, Can. J. Phys. **89**, 47 (2011).
[74] W. Vassen, Ultracold He spectroscopy: QED test, line shapes and nuclear sizes., Talk at FKK 2017, Warsaw, http://ffk2017.fuw.edu.pl/assets/1/3_Vassen.pptx.
[75] P. Mueller *et al.*, Nuclear charge radius of He-8, Phys. Rev. Lett. **99**, 252501 (2007).
[76] E. Riis, A. G. Sinclair, O. Poulsen, G. W. F. Drake, W. R. C. Rowley, and A. P. Levick, Lamb shifts and hyperfine structure in $^6Li^+$ and $^7Li^+$: Theory and experiment, Phys. Rev. A **49**, 207 (1994).
[77] J. K. Thompson, D. J. H. Howie, and E. G. Myers, Measurements of the $1s2s\,^1S_0$–$1s2p\,^3P_{1,0}$ transitions in helium-like nitrogen, Phys. Rev. A **57**, 180 (1998).
[78] C. De Jager, H. De Vries, and C. De Vries, Nuclear charge- and magnetization-density-distribution parameters from elastic electron scattering, At. Data Nucl. Data Tables **14**, 479 (1974).
[79] J. de Vries, D. Doornhof, C. de Jager, R. Singhal, S. Salem, G. Peterson, and R. Hicks, The 15N ground state studied with elastic electron scattering, Phys. Lett. B **205**, 22 (1988).
[80] L. Schaller, L. Schellenberg, A. Ruetschi, and H. Schneuwly, Nuclear charge radii from muonic X-ray transitions in beryllium, boron, carbon and nitrogen, Nucl. Phys. **A343**, 333 (1980).
[81] C. G. Parthey, A. Matveev, J. Alnis, R. Pohl, T. Udem, U. D. Jentschura, N. Kolachevsky, and T. W. Hansch, Precision Measurement of the Hydrogen-Deuterium $1S - 2S$ Isotope Shift, Phys. Rev. Lett. **104**, 233001 (2010).
[82] U. Jentschura, A. Matveev, C. Parthey, J. Alnis, R. Pohl, T. Udem, N. Kolachevsky, and T. Hansch, Hydrogen-deuterium isotope shift: From the $1S - 2S$-transition frequency to the proton-deuteron charge-radius difference, Phys. Rev. A **83**, 042505 (2011).
[83] B. de Beauvoir, C. Schwob, O. Acef, L. Jozefowski, L. Hilico, F. Nez, L. Julien, A. Clairon, and F. Biraben, Metrology of the hydrogen and deuterium atoms: Determination of the Rydberg constant and Lamb shifts, Eur. Phys. J. D **12**, 61 (2000).
[84] B. de Beauvoir, F. Nez, L. Julien, B. Cagnac, F. Biraben, D. Touahri, L. Hilico, O. Acef, A. Clairon, and J. J. Zondy, Absolute Frequency Measurement of the $2S - 8S/D$ Transitions in Hydrogen and Deuterium: New Determination of the Rydberg Constant, Phys. Rev. Lett. **78**, 440 (1997).
[85] C. Schwob, L. Jozefowski, B. de Beauvoir, L. Hilico, F. Nez, L. Julien, F. Biraben, O. Acef, J.-J. Zondy, and A. Clairon, Optical Frequency Measurement of the $2S - 12D$ Transitions in Hydrogen and Deuterium: Rydberg Constant and Lamb Shift Determinations, Phys. Rev. Lett. **82**, 4960 (1999).
[86] M. Weitz, A. Huber, F. Schmidt-Kaler, D. Leibfried, W. Vassen, C. Zimmermann, K. Pachucki, T. W. Hänsch, L. Julien, and F. Biraben, Precision measurement of the 1S ground-state Lamb shift in atomic hydrogen and deuterium by frequency comparison, Phys. Rev. A **52**, 2664 (1995).
[87] J. C. Bernauer *et al.* (A1 Collaboration), Electric and magnetic form factors of the proton, Phys. Rev. C **90**, 015206 (2014).
[88] P. J. Mohr, B. N. Taylor, and D. B. Newell, CODATA recommended values of the fundamental physical constants: 2010, Rev. Mod. Phys. **84**, 1527 (2012).
[89] M. S. Fee, A. P. Mills, S. Chu, E. D. Shaw, K. Danzmann, R. J. Chichester, and D. M. Zuckerman, Measurement of the

Positronium S-131- S-231 Interval by Continuous-wave Two-photon Excitation, Phys. Rev. Lett. **70**, 1397 (1993).

[90] A. Czarnecki, K. Melnikov, and A. Yelkhovsky, Positronium S state spectrum: Analytic results at O(m alpha**6), Phys. Rev. A **59**, 4316 (1999).

[91] B. Holdom, Two U(1)'s and epsilon charge shifts, Phys. Lett. **166B**, 196 (1986).

[92] M. Pospelov and Y.-D. Tsai, Probing light bosons in the Borexino-SOX experiment, arXiv:1706.00424.

[93] M. Pospelov, Secluded U(1) below the weak scale, Phys. Rev. D **80**, 095002 (2009).

[94] P. J. Mohr, D. B. Newell, and B. N. Taylor, CODATA recommended values of the fundamental physical constants: 2014, Rev. Mod. Phys. **88**, 035009 (2016).

[95] I. Angeli and K. Marinova, Table of experimental nuclear ground state charge radii: An update, At. Data Nucl. Data Tables **99**, 69 (2013).

[96] G. W. Drake, *Atomic, Molecular and Optical Physics* (Springer, New York, 2006).

[97] H. A. Schuessler, E. N. Fortson, and H. G. Dehmelt, Hyperfine structure of the ground state of $^3He^+$ by the ion-storage exchange-collision technique, Phys. Rev. **187**, 5 (1969).

[98] S. D. Rosner and F. M. Pipkin, Hyperfine Structure of the 2^3S_1 State of He^3, Phys. Rev. A **1**, 571 (1970).

[99] V. c. v. Patkóš, V. A. Yerokhin, and K. Pachucki, Higher-order recoil corrections for triplet states of the helium atom, Phys. Rev. A **94**, 052508 (2016).

[100] V. Patkóš, V. A. Yerokhin, and K. Pachucki, Higher-order recoil corrections for singlet states of the helium atom, Phys. Rev. A **95**, 012508 (2017).

[101] V. c. v. Patkóš, V. A. Yerokhin, and K. Pachucki, Higher-order recoil corrections for singlet states of the helium atom, Phys. Rev. A **95**, 012508 (2017).

[102] P. Mueller, I. A. Sulai, A. C. C. Villari, J. A. Alcántara-Núñez, R. Alves-Condé, K. Bailey, G. W. F. Drake, M. Dubois, C. Eléon, G. Gaubert, R. J. Holt, R. V. F. Janssens, N. Lecesne, Z.-T. Lu, T. P. O'Connor, M.-G. Saint-Laurent, J.-C. Thomas, and L.-B. Wang, Nuclear Charge Radius of ^8He, Phys. Rev. Lett. **99**, 252501 (2007).

[103] U. D. Jentschura, S. Kotochigova, E.-O. Le Bigot, P. J. Mohr, and B. N. Taylor, Precise Calculation of Transition Frequencies of Hydrogen and Deuterium Based on a Least-Squares Analysis, Phys. Rev. Lett. **95**, 163003 (2005).

[104] P.-L. Luo, J.-L. Peng, J. Hu, Y. Feng, L.-B. Wang, and J.-T. Shy, Precision frequency measurements of $^{3,4}He 2^3P \rightarrow 3^3D$ transitions at 588 nm, Phys. Rev. A **94**, 062507 (2016).

[105] C. Dorrer, F. Nez, B. de Beauvoir, L. Julien, and F. Biraben, Accurate Measurement of the $2^3S_1 - 3^3D_1$ Two-Photon Transition Frequency in Helium: New Determination of the 2^3S_1 Lamb Shift, Phys. Rev. Lett. **78**, 3658 (1997).

[106] P.-L. Luo, J.-L. Peng, J.-T. Shy, and L.-B. Wang, Precision Frequency Metrology of Helium $2^1S_0 \rightarrow 2^1P_1$ Transition, Phys. Rev. Lett. **111**, 013002 (2013).

[107] R. P. M. J. W. Notermans and W. Vassen, High-Precision Spectroscopy of the Forbidden $2^3S_1 \rightarrow 2^1P_1$ Transition in Quantum Degenerate Metastable Helium, Phys. Rev. Lett. **112**, 253002 (2014).

[108] S.-S. Huang, The Continuous Absorption Coefficient of the Helium Atom, Astrophys. J. **108**, 354 (1948).

[109] J. Traub and H. M. Foley, Variational calculations of energy and fine structure for the 2^3P state of helium, Phys. Rev. **116**, 914 (1959).

[110] R. Sack, Generalization of Laplace's expansion to arbitrary powers and functions of the distance between two points, J. Math. Phys. **5**, 245 (1964).

[111] P. Serra and S. Kais, Ground-state stability and criticality of two-electron atoms with screened Coulomb potentials using the B-splines basis set, J. Phys. B **45**, 235003 (2012).